Research Article

Olubukola A. Oni*, Sodiq A. Alimi, Ahzegbobor P. Aizebeokhai, and Henry O. Boyo

Interpretation of aeromagnetic and remote sensing data of Auchi and Idah sheets of the Benin-arm Anambra basin: Implication of mineral resources

https://doi.org/10.1515/geo-2022-0463
received June 28, 2021; accepted February 13, 2023

Abstract: The need for mineral resources for economic development is key in both developing and developed countries. However, miners usually resort to random excavation of mineral deposits without proper investigation to identify structures of interest in target areas. This usually leads to land depletion and abandonment. The aim of this study is to assess the mineral potential in part of the Benin-arm of the Anambra basin by investigating the geophysical characteristics of the area using remote sensing and aeromagnetic data. Surface and subsurface regional structures, including faults and zones of mineralisation, were mapped by integrating aeromagnetic and remote sensing data. The mineral bearing zones that show high prospects of mineral deposits in the region were identified. The rose diagram revealed that the surface lineaments are aligned in the NW–SE, N–S, NE–SW, E–W, NNE–SSW, ENE–WSW, and ESE–WNW directions. The orientations of the subsurface lineaments are aligned mostly in the NE–SW, N–S, and E–W directions. The magnetic intensity ranged between −431.38 and 399.82 nT, while reduction-to-pole magnetic intensity ranged from −416 to 664.45 nT. The first vertical derivative showed magnetic intensity which ranged from −0.5863 to 0.9060 nT/km^2. The total horizontal derivative magnetic intensity ranged from −0.00031 to 0.762691 nT/km^2, while the analytic signal showed magnetic intensity ranging from 14.0664 to 394,607.3438 nT/cm^2. The windowed Euler deconvolution depth to magnetic source showed depth range of <20 to 2,000 m. Many of the features delineated in the study area were characterised by shallow magnetic source depths (<500 m); this is a common characteristic of basement complex terrains. Deeper magnetic source depths (>1,000 m) were observed in the sedimentary terrain. Mineral exploration should be focused in areas with high lineament concentration, as lineaments are potential conduits for economic minerals deposition.

Keywords: lineament, magnetic, subsurface, geologic, fault, structure, surface, exploration, mineral

1 Introduction

In both developing and developed countries, the need for mineral resources for economic growth is crucial. As a result, more attention is being placed on harnessing mineral resources aside from oil and gas to support the recovery of the country's economic growth [1–4]. In many developing countries, including Nigeria, the mining of mineral resources is of paramount importance [3]. Nigeria is endowed with abundant natural resources that have added enormously to the socio-economic benefits and wealth of the country [5]. However, the greatest difficulty in the development of large-scale mining is the lack of a comprehensive understanding of the geophysical characteristics of the region. Thus, miners sometimes result in random excavation of mines in their effort to locate primary deposits. This exposes several non-mineralised areas that would have been used for agricultural purposes to large scale land depletion and abandonment. Consequently, significant and economic mining activities require a comprehensive understanding of the geophysical characteristics of the region. Although mineral resources are essential sources of wealth for a country and need to be explored, mined, and processed before they can be of value, these processes are capital intensive. Extensive

* **Corresponding author: Olubukola A. Oni,** Department of Physics, Covenant University, P.M.B 1023, Ota, Ogun State, Nigeria, e-mail: aina.onipgs@stu.cu.edu.ng
Sodiq A. Alimi: Department of Geology, University of Ilorin, Kwara State, Nigeria
Ahzegbobor P. Aizebeokhai: Department of Physics, Covenant University, P.M.B 1023, Ota, Ogun State, Nigeria
Henry O. Boyo: Department of Physical and Chemical Sciences, Elizade University, Ilara Mokin, Ondo State, Nigeria

geological information is required for effective exploration; this would reduce the cost of exploration. This extensive analysis requires the use of geophysical methods. Therefore, this study is an assessment of the mineral resource potential in part of the Benin-arm of the Anambra basin using aeromagnetic and remote sensing data.

1.1 Detailed geology of the study area

The study area covers Auchi and Idah of the Benin-arm of the Anambra basin (Figures 1 and 2). The area mostly covers the northern part of Edo state, extending into the southern part of Kogi state, Nigeria. The area lies within the geographical coordinates of latitude 7°0′0″ and 7°30′00″ North and longitude 6°0′0″ and 6°60′0″ East. The climate is tropical and humid; the temperature varies from 42°C in February to 23°C in July. The area is marked by two distinct seasons: the dry and rainy seasons. The dry season spans between late September and early April, while the rainy season is between late April and early September. The Anambra Basin is one of Nigeria's Cretaceous sedimentary basins [6,7]. The basin is bounded by the Niger Delta Hinge Line on the south–western flank, the Benue Flank in the north–west, and the Abakaliki fold belt in the south–east [6]. The southern frontier of the basin overlaps with the northern frontier of the Niger Delta basin [8].

The basin is coarsely triangular in shape, which covers an approximate area of 40,000 km^2 in which the sediment thickness aggregates southwards to a maximum thickness of 12,000 m in the central fragment of the Niger Delta region [6,8]. The Anambra basin stretches from the southern part of the confluence of the west of the River Niger and Benue through terrains like Asaba, Okene, Auchi, Agbo, and to the east of the river Awka, Idah, Onitsha, Nsukka, and Anyangba area. The Udu-Idah cliff slopes slightly in the southwest direction into the flood plain of the River Niger and across to the west at an elevation of about 300 m [9]. The basin is mainly drained by the Anambra River and its main tributaries, the Mamu and Adada [9].

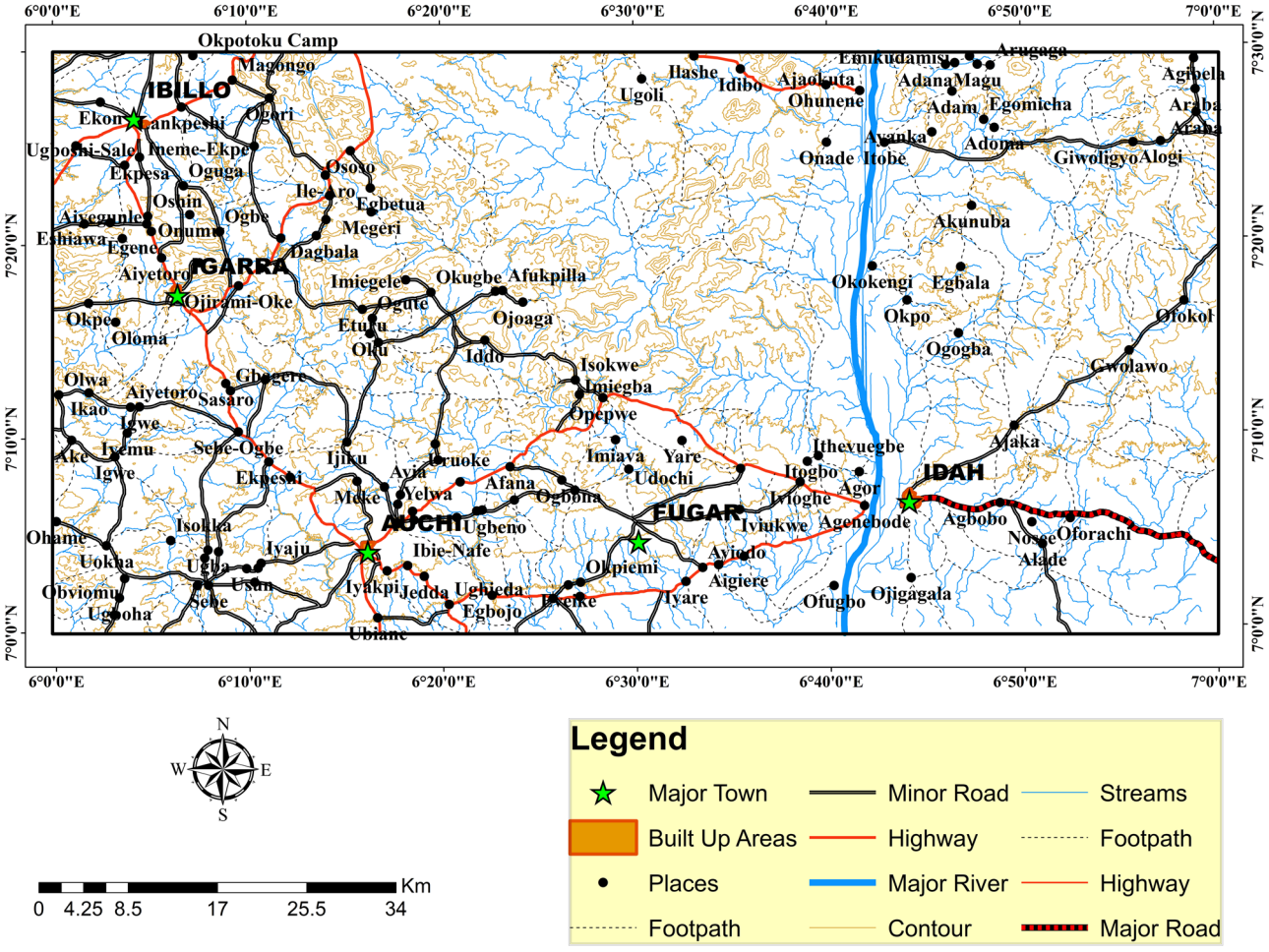

Figure 1: Map of the study area (Auchi and Idah).

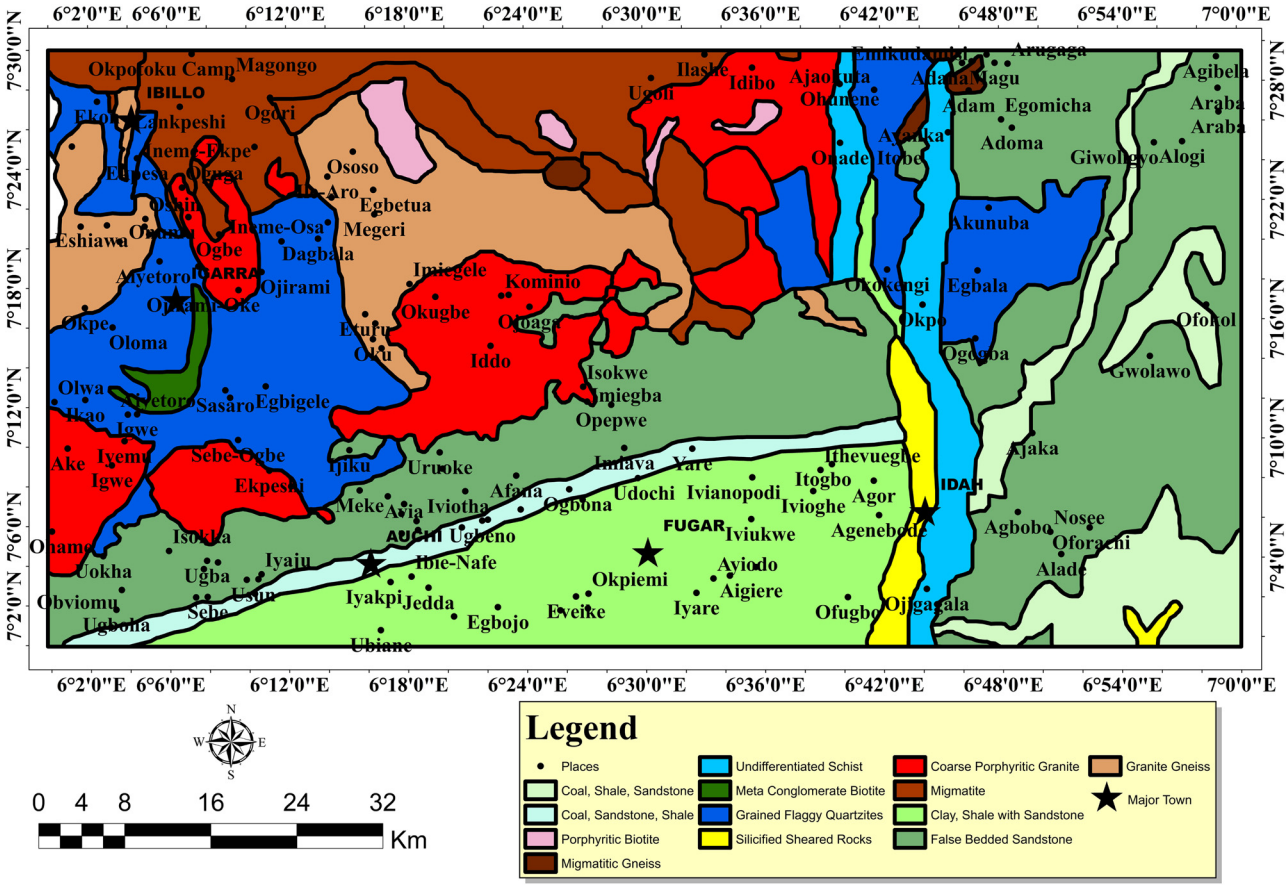

Figure 2: Geological map of the study area.

2 Methods

The methods deployed in this study include the aeromagnetic and remote sensing methods. The raw aeromagnetic data of sub-nanotesla resolution scale was obtained from the Nigerian Geological Survey Agency.

The Landsat8 image (Path/Row-191/054) resolution of 30 m was provided by the United States Geological Survey in collaboration with the National Aeronautics and Space Administration. Using the Operational Land Imager sensor, the Landsat image was captured on February 4, 2014, at 10:03:33 am with the solar elevation angle at 52.14° and the azimuth of the sun at 130.8°.

2.1 Aeromagnetic data processing

To process the aeromagnetic data, two databases were created using the magnetic data processing software by Oasis Montaj Geosoftware 7.0. The data processing consists of four procedures, which are gridding, determination of the residual magnetic field by subtracting IGRF from total magnetic data measured from the field, micro-levelling of the whole dataset to eliminate any form of errors [10,11], and integration of the different windows for each different type of data using different filtering techniques expressed in equations (1)–(3).

Interpretation was carried out by inspecting the total magnetic field. The residual map was generated after the removal of regional effects from the total magnetic intensity using the Butterworth low-pass filtering method. Butterworth helped in simplifying the filter by using a normalised low-pass polynomial. The residual anomaly maps are derived using polynomial fitting to desirable degrees. Polynomial fitting degrees 1 and 2 were used to generate residual anomaly maps and to investigate how the degree of polynomial fitting affects the appearance of the maps. The equation used in the algorithm for the separation of the regional field is expressed as follows:

$$r = a_0 + a_1(X - X_{\text{ref}}) + a_2(Y - Y_{\text{ref}}), \quad (1)$$

where r represents the regional field, a_0, a_1, and a_2 are known as the regional polynomial coefficients, and X_{ref} and Y_{ref} are the X and Y coordinates of the geographic

centre of the dataset, respectively. X and Y offsets are used to prevent higher order coefficients from being very small in the polynomial equation. The residual magnetic intensity (RMI) data were processed to improve the signal-to-noise ratio and eliminate any high frequency events that may reflect cultural or other noise types or error in the data and are then subjected to further processing. Only the residual fields are of concern and thus form the basis of this study. Various filters such as reduction-to-pole (RTP), vertical derivative, analytic signal, and Euler deconvolution were used for the aeromagnetic processing.

RTP algorithm was applied to the total magnetic anomaly because the data were acquired closer to the magnetic latitude. The RTP map was produced by applying RTP filter on the RMI map using Fast Fourier Transform (FFT). The RTP operation in wave number domain can be represented as follows:

$$A_{\mathrm{p}}(u, v) = \frac{A_{\mathrm{e}}(u, v)}{(\sin I + i \cos I \cos (D - \theta))^2}, \tag{2}$$

where $A_{\mathrm{p}}(u, v)$ is the Fourier transform of the observed magnetic data, $A_{\mathrm{e}}(u, v)$ is the Fourier transform of the vertical magnetic field, I is the inclination, D is the declination of the core field, (u, v) is the wave number corresponding to the (x, y) directions, respectively and $\theta = \arctan\left(\frac{u}{v}\right)$ [12]. Since the data were collected near the magnetic equator, RTP algorithm was applied to the total magnetic anomaly.

The parameters involved include an inclination value of −11.27 and a declination value of −1.18. An amplitude correction value of 60 was also applied to reduce latitudinal effects because the survey was carried out in an area close to the equator, hence RTP at low latitude.

The RTP grid data were subjected to a first vertical derivative (FVD) filter. The FVD filter allows small and large amplitude responses to be more equally represented. The FVD grid helps enhance linear features in the area. Vertical derivative filters are generally applied to gridded data using FFT filters. These maps were produced by the application of derivative filters on the RTP map of the area of study using FFT. An upward continuation value of 200 was also applied to the filter in order to reduce the influence of signatures that may be due to manmade features. Different vertical derivatives of the magnetic fields can be measured through multiplication of the field's amplitude spectra by a factor in the form as follows:

$$\frac{1}{n}[(u^2 + v^2)^{1/2}]^n, \tag{3}$$

where n is the order of the vertical derivative and (u, v) is the wave number corresponding to the (x, y) directions, respectively. The use of the first horizontal gradient or derivative (1HD) was used to enhance the RTP grid and is important for mapping linear geological structures such as faults in the magnetic data.

The analytic signal behaves like the RTP filter. It actually takes the magnitude of the square root of the vertical and horizontal components of the magnetic responses [13]. This processing enhancement was used in mapping the edges of the permanently magnetised sources and for centering anomalies over their causative bodies in areas of low magnetic latitude but does not depend on the direction of magnetisation. The analytic signal map was created via the application of an analytic signal filter on the RMI map of the area of study. The extension of the Geosoft Oasis Montaj's depth to basement, which defines the location (distance along the profile and depth), dip (orientation), and intensity (susceptibility) of magnetic source bodies for magnetic profiles, was used in an attempt to measure the depth to basement of the magnetic bodies in the study area. In calculating the depth of the magnetic anomaly, the Euler deconvolution function, which makes use of both the horizontal and vertical derivatives, was employed.

The Euler deconvolution function assumes that the source body is either a dyke or contact of limitless depth and employs the least-square method in a series of shifting the profile windows to solve for source body parameters [14]. Solutions deduced from total field profile are referred to as "Dyke" solutions, while solutions resulting from horizontal gradient are referred to as "Contact" solutions. Euler deconvolution algorithm was used for the location and depth determination of causative anomalous bodies from gridded aeromagnetic data. The 1.0 and 2.0 values of the structural index (N) were used based on individual dykes and sills models of the source [15]. Through the application of the window method, the solutions derived were further refined to eliminate ambiguity. This was accomplished by limiting the solutions obtained from Euler deconvolution to a maximum tolerance depth of 10% while rejecting the uncertainty in depth (dz in percentage) that is greater than 10% just for easy processing. Likewise, horizontal (dx in percentage) uncertainty has been fixed at 20%. This automatically appends a mask to those solutions whose outputs do not fall within the stated window.

2.2 Landsat 8 processing

The image processing software Environment for Visualising Images (ENVI) version 5.1 was used for processing the remote sensing data. The remote sensing data were

interpreted using ArcGIS, Rockware, PCI Geomatic software, Rockworks, and GeoRose software. Atmospheric correction was applied to the Landsat8 scenes using the Fast Line-of-sight Atmospheric Analysis of Spectral Hypercube (FLAASH) algorithm [16]. The FLAASH algorithm was implemented using the Sub-Arctic Summer atmospheric and maritime aerosol models [13]. During the atmospheric correction, raw radiance data from the imaging spectrometer were re-scaled to reflectance data.

Colour composite images were produced based on known spectral properties of rocks and alteration minerals in relation to the selected spectral bands. Bands 4, 3, and 2 were used to produce true colour composite, while bands 5, 4, and 1 were used to produce false colour composite images of the study area for lithological mapping. Both the true and false colour maps were produced by importing individual 8-bit greyscale surface reflectance bands of the Landsat8 data into the ENVI workspace. This was applied after the Landsat8 data for the area had been processed and corrected using ENVI and ArcGIS software. Band ratio indices were developed and implemented to Landsat8 spectral bands for mapping poorly exposed lithological units, geological structures, and mineral alteration in the study area. Spectral-band ratio indices were used to map the spectral signatures of iron oxide/hydroxide minerals, the OH– and Fe, and Mg–O–H bearing lithological units within the area of study. The surface and subsurface lineaments were merged in ArcGIS to get a detailed understanding of the lineament structure or lineament pattern of the research area. Two band ratios were formed based on the laboratory spectral of minerals for mapping the abundance of iron oxide/hydroxide minerals in rocks using the Landsat8 bands [17,18]. Goethite, jarosite, hematite, and limonite are typically heavily absorbed into visible and near-infrared (0.4–1.1 μm), coinciding with Landsat8 bands 2, 3, 4, and 5, and high reflectance into short wave infrared (SWIR) (1.56–1.70 μm) coinciding with Landsat8 band 6 [19]. Therefore, band ratio of 4/2 was used to map iron oxide mineral groups. The Landsat8 SWIR bands were used to detect hydroxyl-bearing (Al–OH and Fe, Mg–OH) groups within the study area. Clay minerals contain 2.1–2.4 μm spectral absorption features and 1.55–1.75 μm reflectance, coinciding with Landsat8 band 7 (2.11–2.29 μm) and band 6 (1.57–1.65 μm) [19]. Therefore, ratio 6/7 was used to map the hydroxyl-bearing mineral group in this study. For the ferromagnesium (Fe, Mg–OH) group of minerals, bands 5 and 6 of Landsat8 were used due to the group's high absorption feature in band 5, and low absorption characteristics in band 6.

For a detailed structural and lithological mapping of the study area, surface structures were extracted from processed Landsat8 data of the area using the automatic

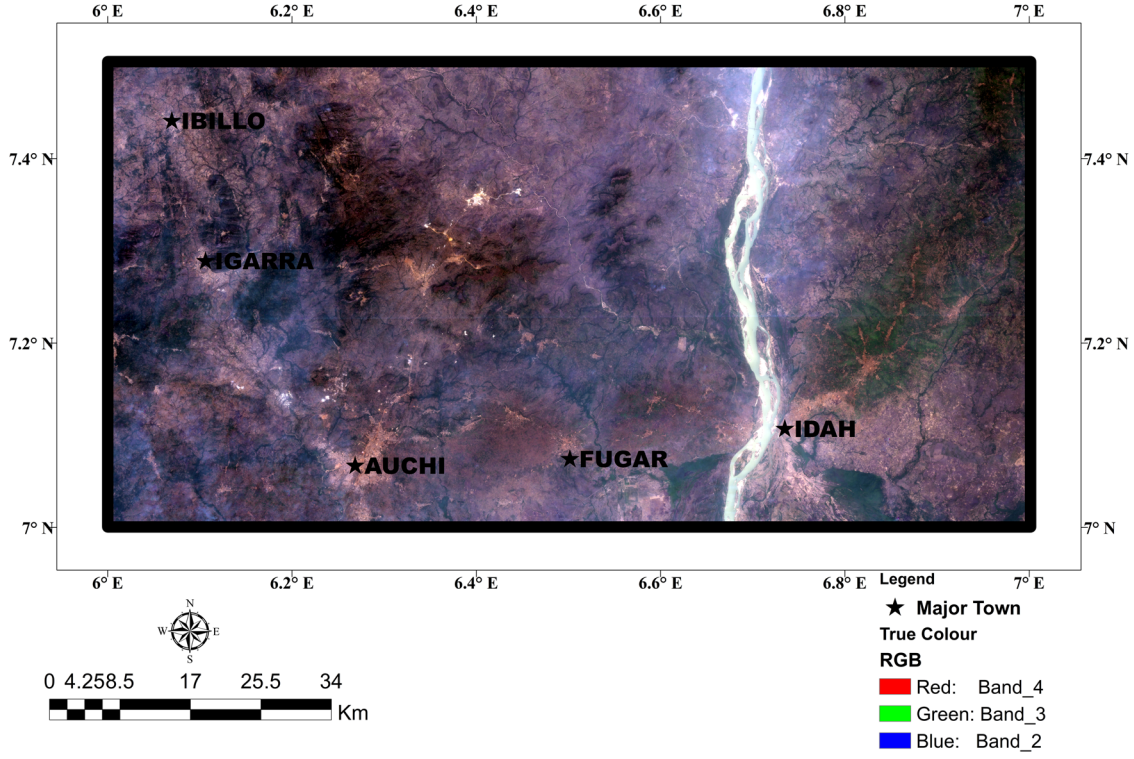

Figure 3: True colour composite (bands 4, 3, and 2) map of the study area.

lineament extraction tool in PCI Geomatica. The lineament density map was produced by combining both the surface and subsurface lineaments and calculating their densities using the line density tool. The surface and subsurface lineaments were merged in ArcGIS to aid a detailed understanding of lineament structure or lineament pattern in the study area.

3 Results

Figures 3 and 4 show the true and false colour composite maps of the area, respectively. The vegetation area appears as dark green on the true composite map, while the false composite map appears red. Human settlements appear light brown on both maps while the major river, which appear white on the true map, appear with a shade of cyan and white colouration on the false map. Areas with different geological or topographical settings are mostly seen in the upper western part of the area; these areas are mostly underlain by basement complex rocks. Igarra's granite plutons of Somorika and Ojirami appear dark brown, while granite gneiss and migmatitic terrains appear brown. The eastern and southeastern parts of the study area are underlain with sedimentary rocks, which include sandstone and shale. These rocks underlie the relatively flat surface and cannot be easily identified in the true colour composite image on a regional scale. Schist and migmatite in the Ugoli and Ajaokuta areas show clearly on the false colour composite map compared to the true colour composite map. Figure 5 shows areas with blue pixels in a grey shade for easy identification; the bright coloured areas represent high reflectance of ratio 6/7. Within the study area, carbonate rocks such as marble are present, and alteration products of such rocks include clay minerals. The green pixels represent areas with ferrous iron-bearing minerals such as olivine, pyroxene, and amphiboles (Figure 5), rocks such as schist and metaconglomerate in the study area host these minerals. The red pixels represent areas dominated by ferric-bearing minerals such as goethite, hematite, and jarosite (Figure 5). Figure 6 shows a greyscale map of band four divided by band two (4/2) for iron oxide alteration mapping. Figure 7 shows the greyscale map of band five divided by band six (5/6) for Fe and Mg–OH bearing lithological units, and Figure 8 shows the greyscale map of band six divided by seven (6/7) showing areas where OH-bearing clay alterations are present in the study area. Figure 5 shows the band ratio map of the area of study. Band ratios of 4/2, 6/7, and 5/6 boost minerals such as clay (pyllosilicates), ferrous, and iron oxides, respectively [20]. The colour composite image of these band ratios can be used

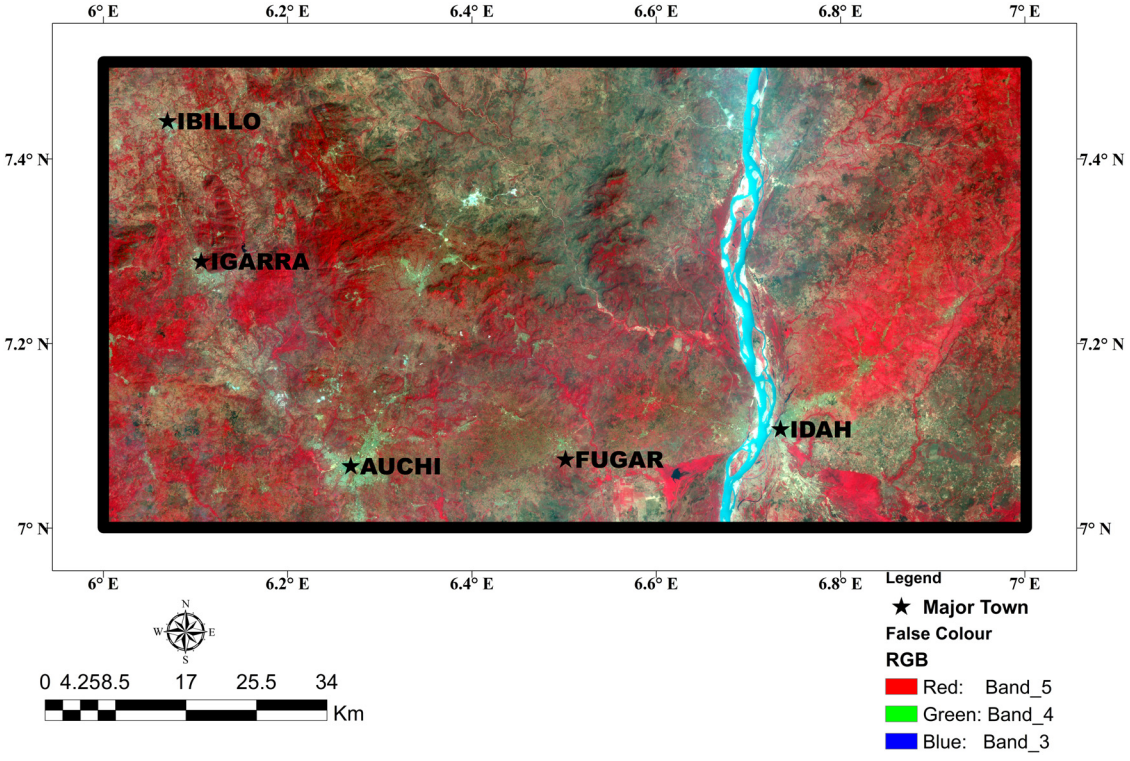

Figure 4: False colour composite (bands 5, 4, and 3) map of the study area.

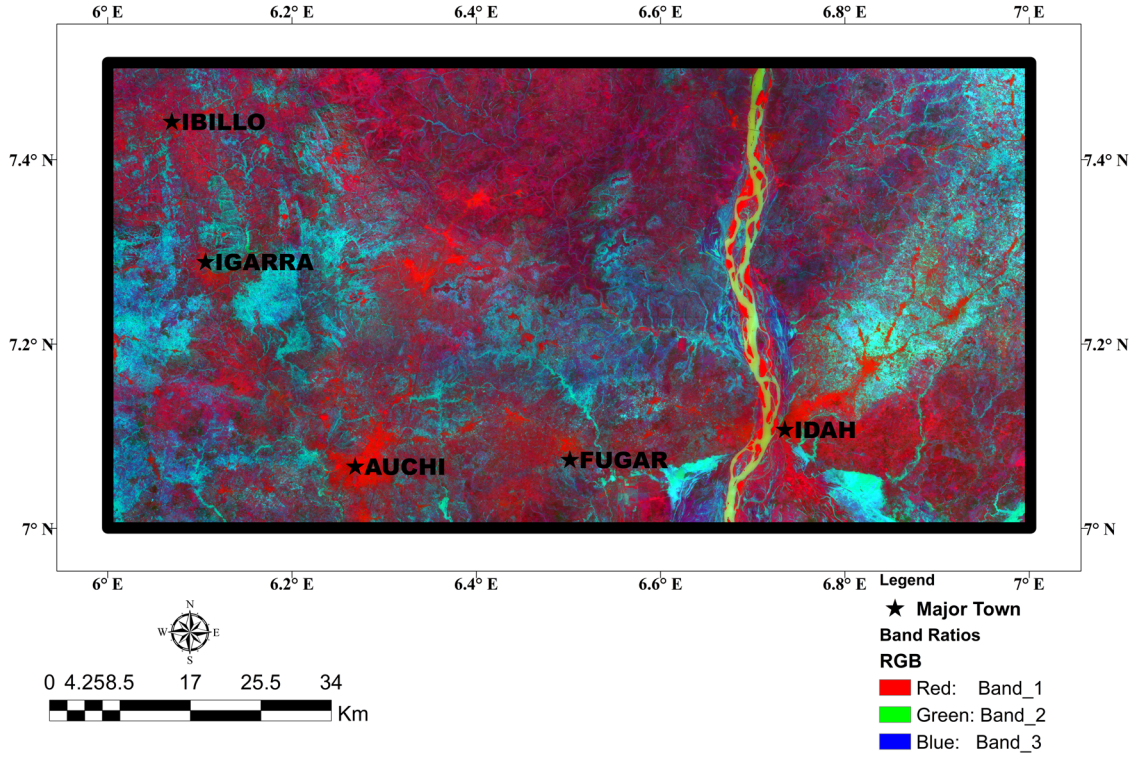

Figure 5: Band ratio map of the study area.

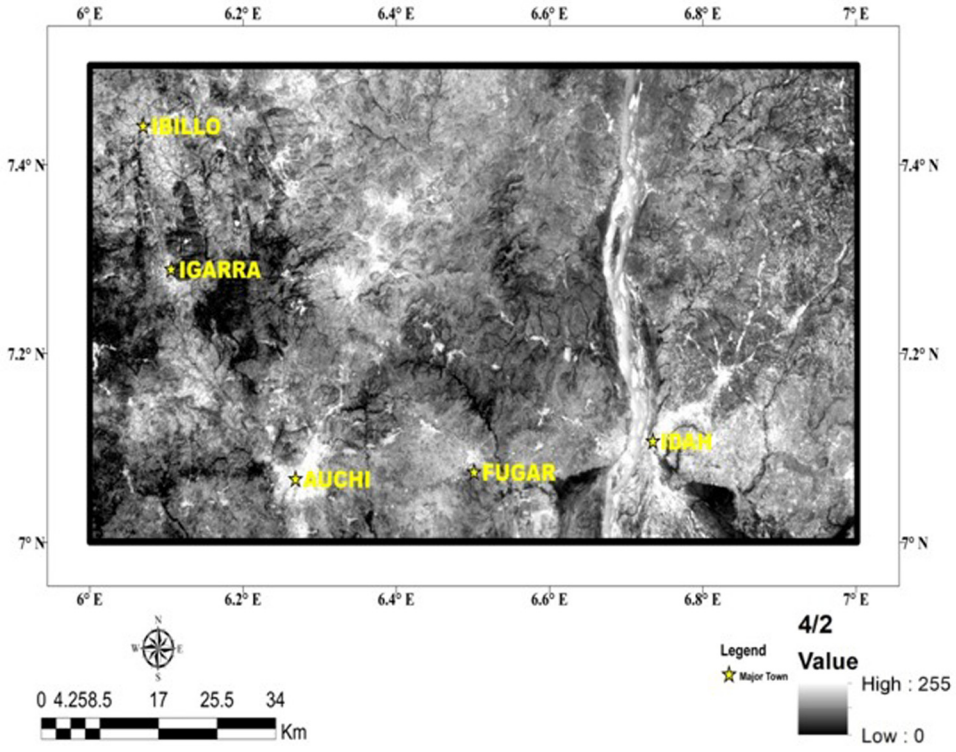

Figure 6: Ratio 4/2 (ferric-ion bearing) map of the area of study.

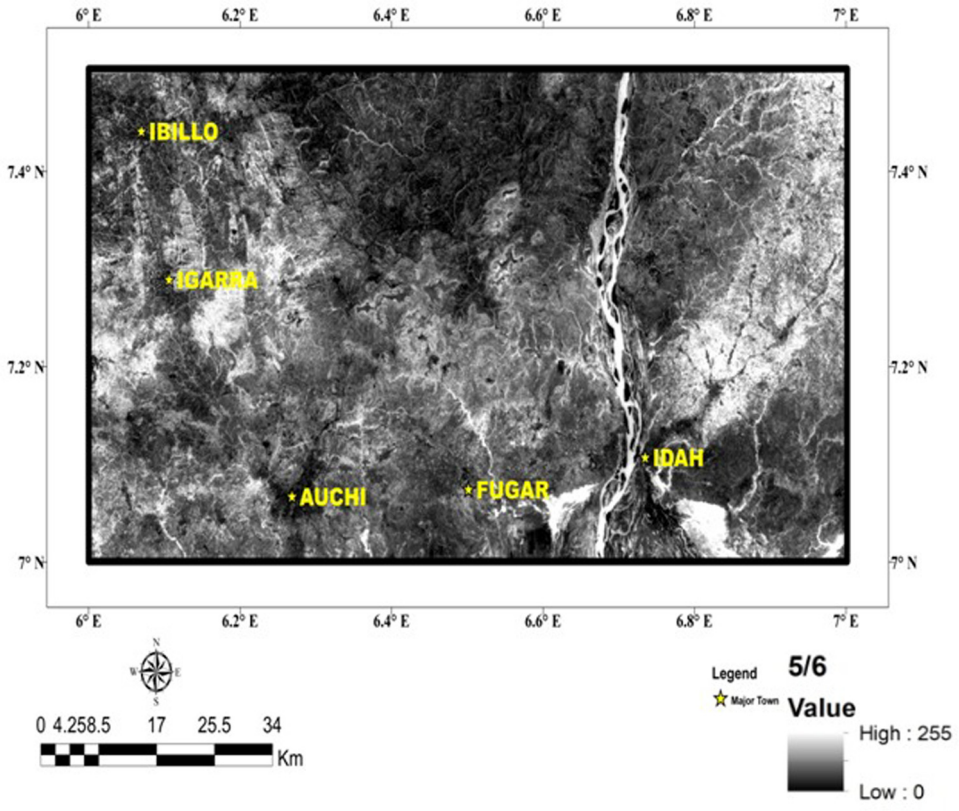

Figure 7: Ratio 5/6 (ferrous-ion bearing) map of the area of study.

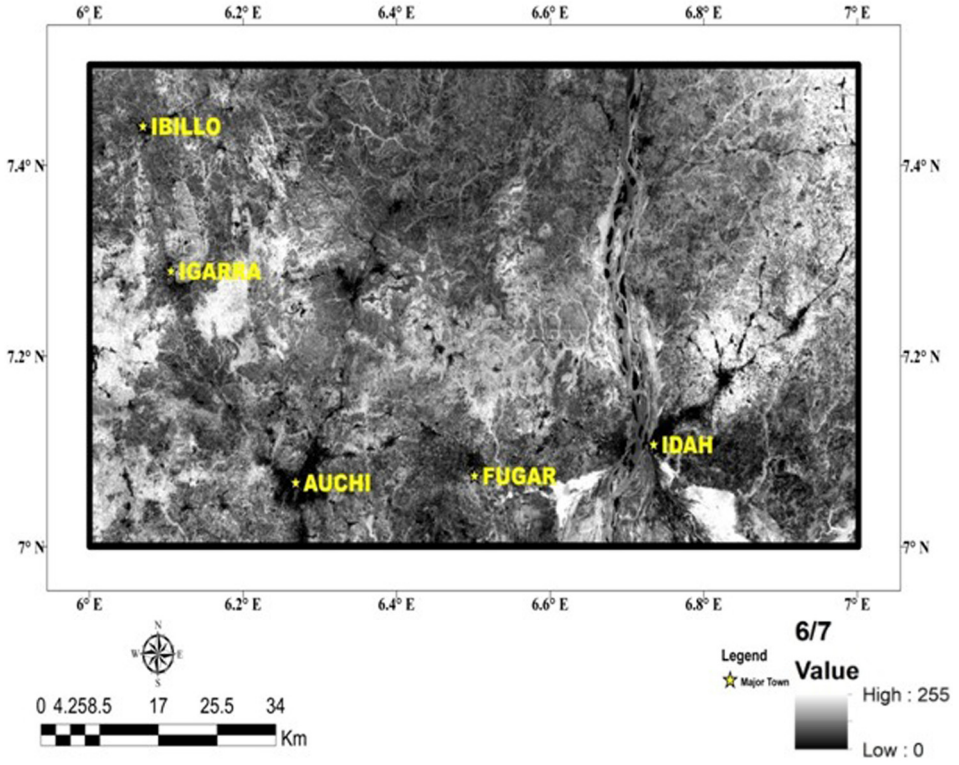

Figure 8: Ratio 6/7 (OH bearing) map of the area of study.

to identify basement complex rocks such as granite, gneiss, basic igneous rocks, and arkose in the study area. Clay/kaolinite can be obtained from the weathering of feldspar-bearing arkose, gneiss, and granite; most schist and sedimentary rocks in the study area contain clay-bearing soils. Biotite bearing quartzite, gneiss, and granite can easily weather into iron oxide. Iron oxide alterations appear to be the most dominant form of alteration in the study area; this may be due to the constant interaction between exposed rocks and weathering agents such as wind and water.

Figure 9 shows extracted surface lineaments in the study area. The displayed lineaments represent geologic structures such as faults, joint-sets, fractures, and lithologic boundaries in the study area. In both the sedimentary and basement complex terrains, minerals are believed to be structurally controlled and the ability to identify these structures provides more information towards preparation of mineral activities. Therefore, the various surface linear features such as faults, joints, fractures, foliations, and river channels that are obvious on the surface were carefully mapped out. It can be seen that surface lineaments are well dispersed within the research area. Both the basement and sedimentary terrains show surface lineaments.

Figure 10 shows the orientation of surface lineaments within the study area. The lineaments are aligned in the NW–SE, N–S, NE–SW, E–W, NNE–SSW, ENE–WSW, and ESE–WNW with a dominant direction towards NNW–SSE, which is similar to the orientations that have been reported earlier [21,22]. Also, the study by Ogbe et al. [21] showed that joints within Igarra and environs trend in the NE–SW to E–W direction. Ajigo et al. [22] also reported NNW–SSE

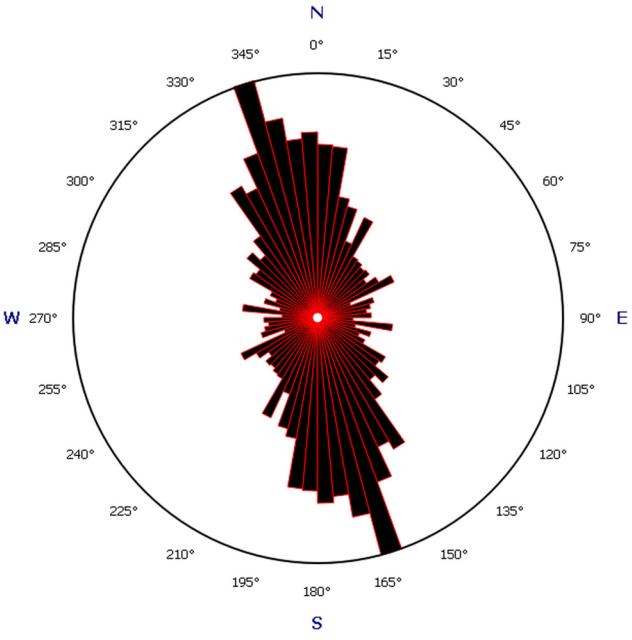

Figure 10: Plot of the general bearing of the surface lineaments.

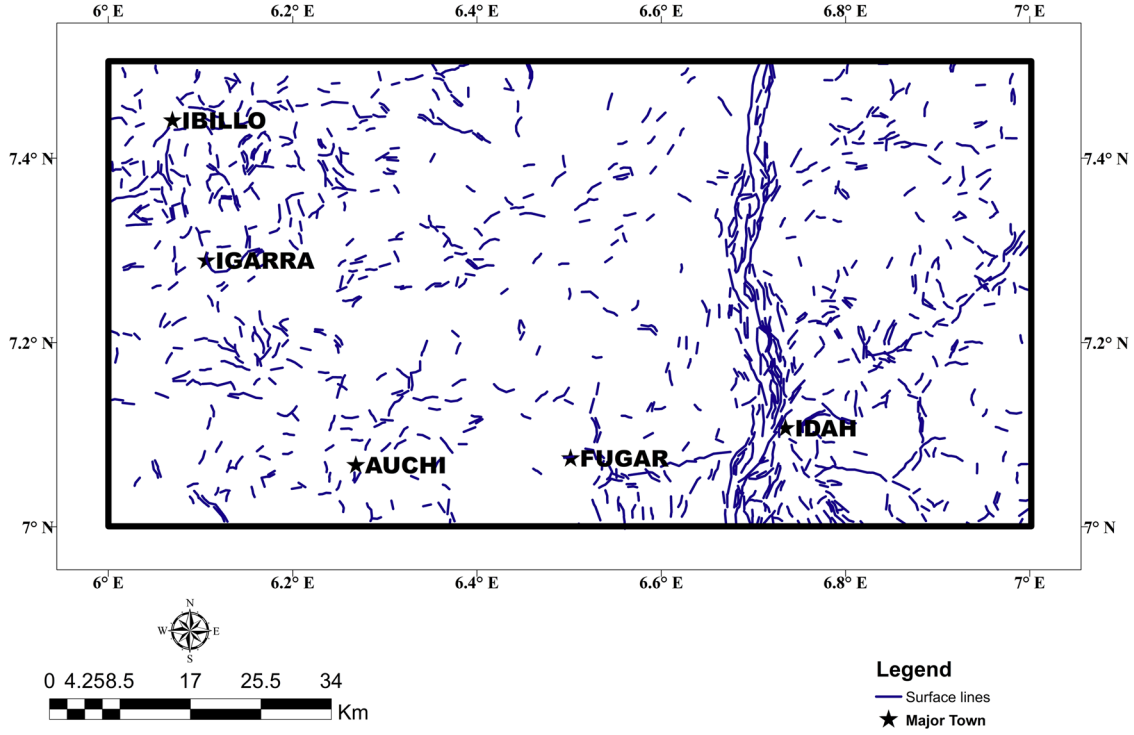

Figure 9: Surface lineaments present in the area of study.

and ENE–WSW as the dominant directions for both foliations and lineaments in the Ibillo-Okene area.

4 Aeromagnetic results

Figure 11 shows the total magnetic intensity map, Figure 12 shows the regional map, and Figure 13 shows the RMI map. The high magnetic intensity zones fall within the basement complex terrain with rocks that are rich in magnetic minerals. Examples of these rocks include basic igneous and metamorphic rocks such as schist, gneiss, dolerite, migmatite, granodiorite, and basalt. The low magnetic intensity values originate from the sedimentary areas covered by materials with low magnetic minerals. Such materials include shale, limestone, sandstone, mudstone, and alluvial sands. Magnetic intensity values within the study area ranged between −431.38 nT for magnetic low and 399.82 nT for magnetic high.

Figure 14 shows the RTP map of the study area. The RTP map showed the magnetic intensity ranging from −416 to 664.45 nT. The sedimentary terrain in the eastern and southern parts of the study area shows low to moderate magnetic intensities, while the basement terrain in the western and north-western parts of the study area displays high magnetic intensities. Schists, migmatite, and gneiss are known to be rich in magnetic minerals compared to sandstone, mudstone, shale, and limestone in the area. Figure 14 shows a clear and distinct difference between the basement and sedimentary terrain. The sedimentary terrain appears smooth while the basement terrain appears rough. This is due to the geology of the area, the formation of rocks and the deformation that the rocks in the area have gone through.

Figure 15 shows the FVD map of the area of study, while Figure 16 is the total horizontal derivative map of the study area. Both Figures 15 and 16 show subsurface lineaments such as faults present in the study area. It can be shown that the majority of the subsurface lineament appears in the basement terrain, while few of these lineaments are present in the sedimentary terrain. Figure 15 shows clearly that the complexity of structures within the basement terrain areas is a reflection of the various cycles of deformation that these rocks have undergone. The structures within the sedimentary terrains are dykes that have intruded into the sedimentary basins. A clear visualisation of the extracted lineaments, lithological boundaries, and geological structures such as folds is shown in Figure 17. Figure 18 shows the orientation of the subsurface structure, which aligns mostly in the NE–SW, N–S, and E–W directions. Figure 19 shows the lineament density map, whose density values range from 0 to 1.82. This map shows areas in which lineaments are concentrated. From the lineament density map, areas with high lineament concentration appear in orange colouration with a lineament value

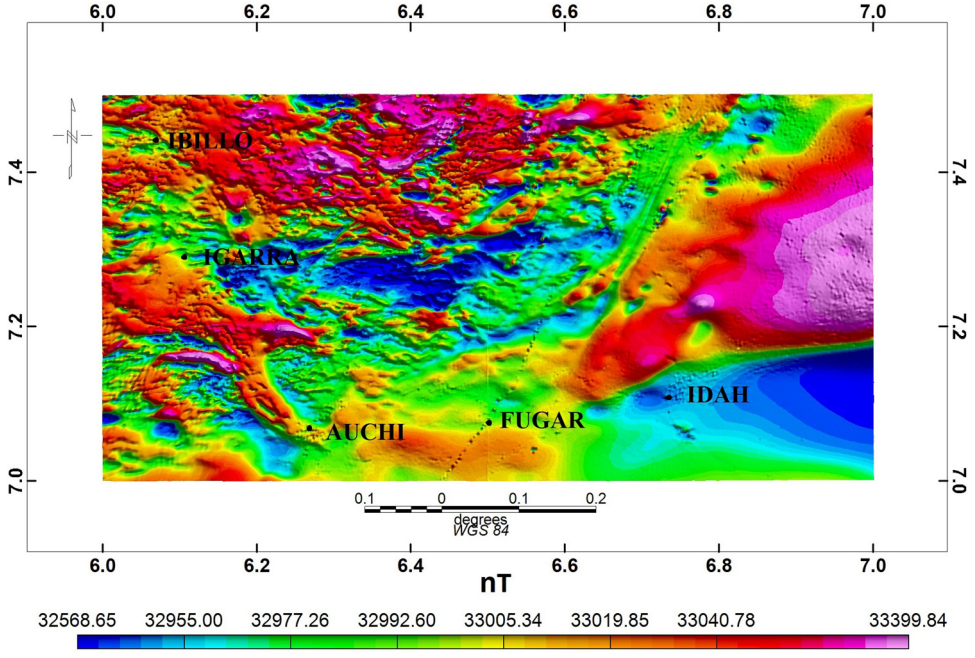

Figure 11: Total magnetic map of the study area.

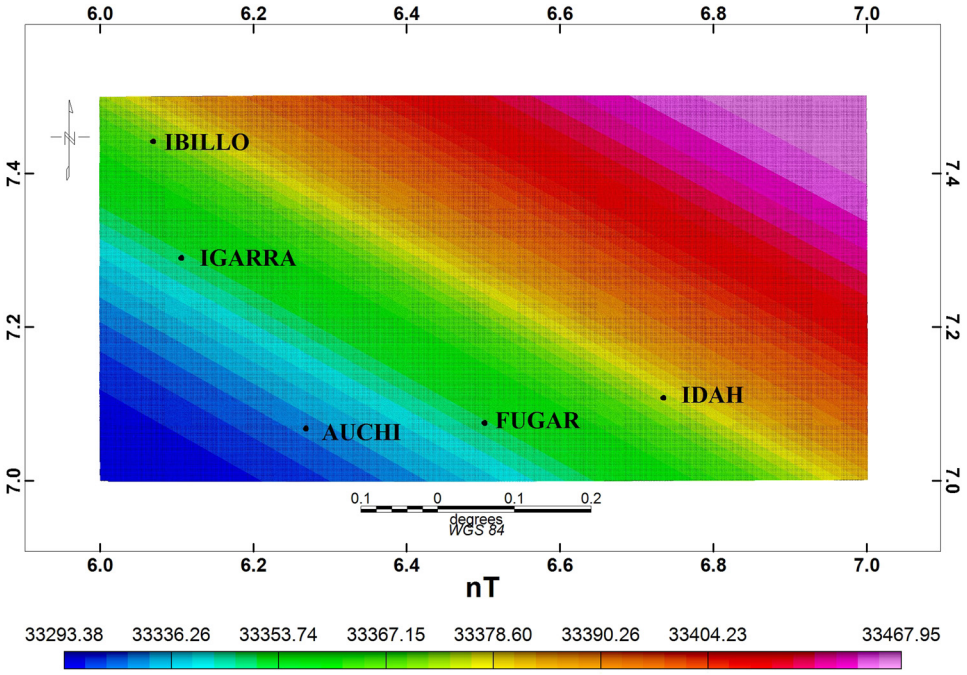

Figure 12: Regional map of the study area.

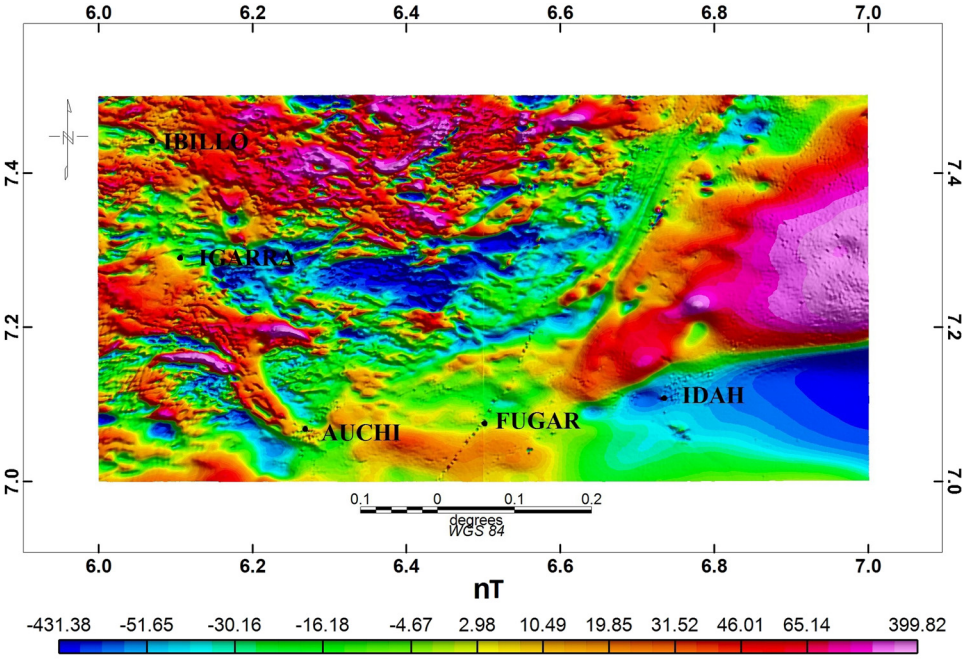

Figure 13: RMI map of the study area.

ranging from 1.01 to 1.82, while areas with moderate lineament concentration appear in yellow with a lineament value ranging from 0.32 to 0.6. Areas with low lineament concentration appear as areas with greenish colouration, with lineament values ranging from 0 to 0.12. Mineral exploration activity should be focused on these high lineament concentration areas due to the fact that lineaments serve as conduits of economic mineral deposits in rocks.

The analytic signal map of the study area is shown in Figure 20. The analytical map showed magnetic intensity ranging from 14.0664 to 394607.3438 nT/cm^2. It indicates

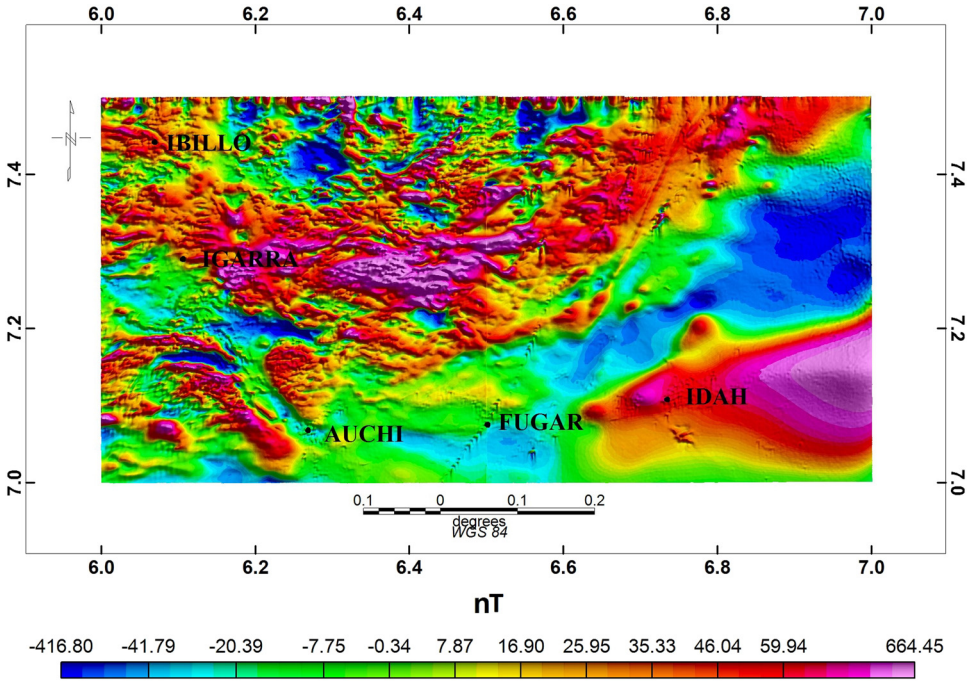

Figure 14: RTP (at low latitude) map of the study area.

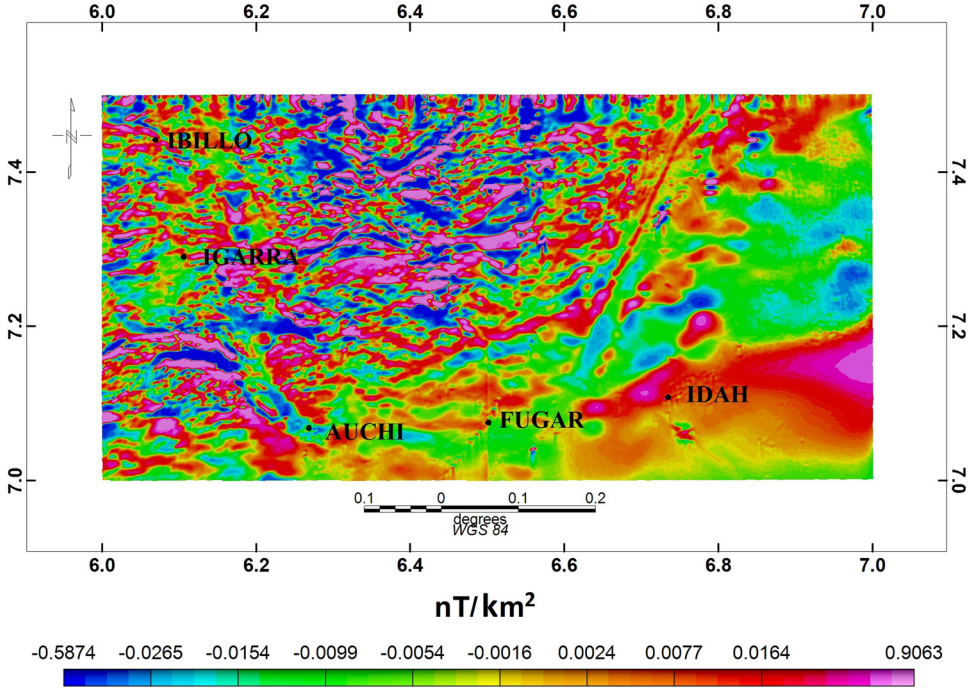

Figure 15: FVD map of the study area.

clearly the sources of the magnetic anomalies. The igneous and metamorphic rocks in the basement terrain are the sources of the magnetic anomalies in the area of study. On the other hand, the sedimentary terrain shows low magnetic intensity signatures except in areas where dykes exist.

Various Euler depths of 100, 500, 1000, and 2,000 m calculated for the study area are shown in Figures 21–24.

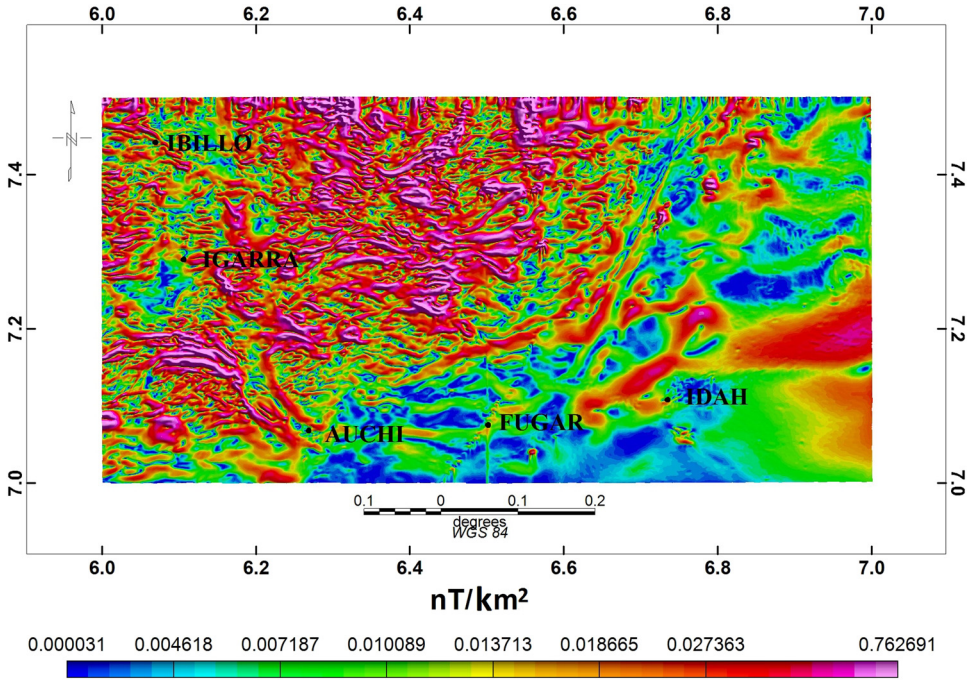

Figure 16: Total horizontal derivative map of the study area.

It can be observed that shallow magnetic depths are common in the basement complex terrains, while deeper depths are seen in the sedimentary terrain. This is to be expected as the bedrock in the basement complex terrain is only overlain by a relatively thin overburden, while piles of sediment over the basement (bedrock) in the sedimentary area are very thick in comparison. Previous studies [23–25] carried out in the Anambra basin agreed with the results of the present study and indicated that shallow depth sources are common in basement complexes, while deeper depth sources are observed in sedimentary terrains.

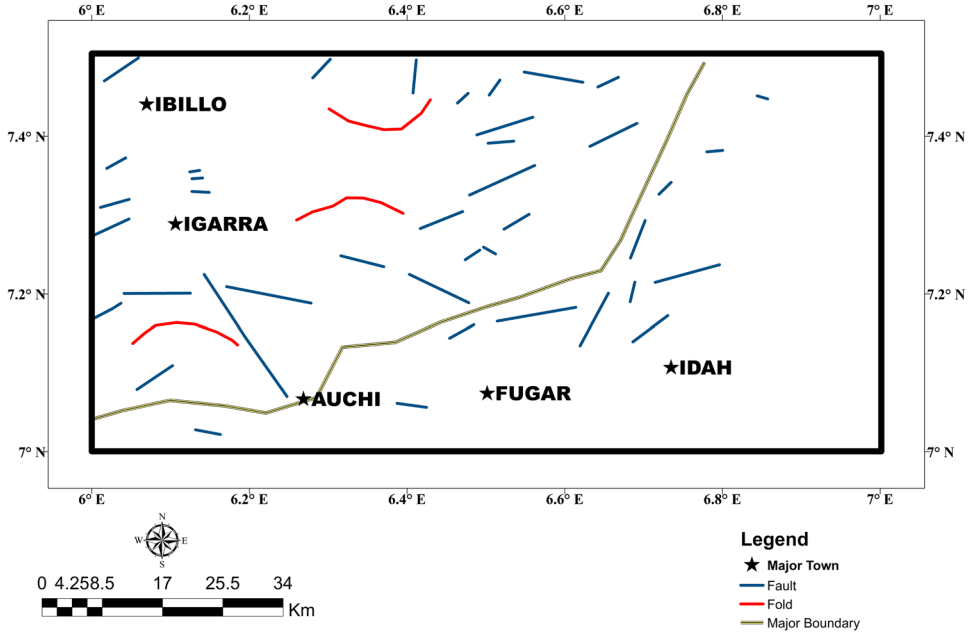

Figure 17: Vectorised subsurface lineaments of the area of study.

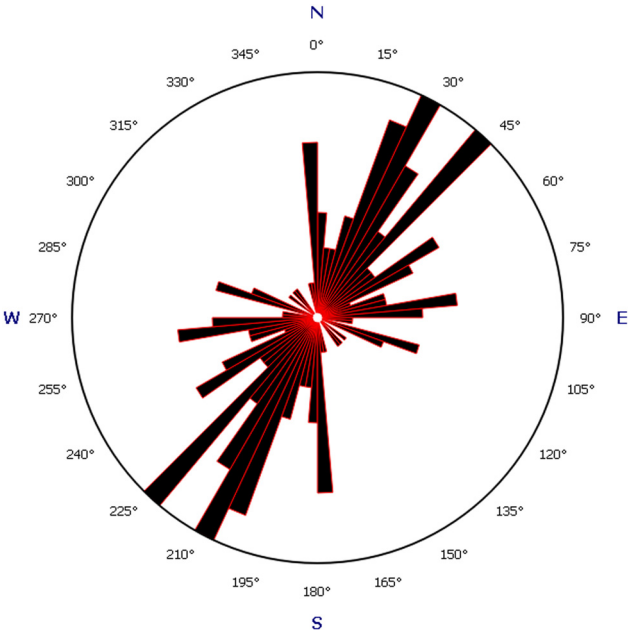

Figure 18: Plot of the general bearing of the subsurface lineaments.

5 Discussion

5.1 Implication for mineral resources

This aim of this study was mapping the lithology and structure of sheets 266 and 267. The objectives of the study are to map out the various lithologies and structures present in the area and assess their potential for mineral exploration. Mineralised pegmatite vein, which are often easily weathered due to the effect of water on feldspar [26], appear to produce clay-like signatures on the band ratio maps. The ability to find such areas helps in easily detecting veins, which can play a major role to host minerals of economic benefit. Also, gold mineralisation has often been discovered in areas within the iron oxide alteration zones [26]. These outcomes provide focus on knowledgeable objectives for better preparation before exploration, rather than random excavation that can lead to waste of resources, time, and money. The lineament map shows areas of high, moderate, and low lineament density. The presence of lineaments shows that the area has the potential to host mineralisation because lineaments can potentially serve as conduits through which hydrothermal alteration can occur. The result from the rose diagram revealed that the surface lineaments are aligned in the NW–SE, N–S, NE–SW, E–W, NNE–SSW, ENE–WSW, and ESE–WNW. The orientations of the subsurface lineaments align mostly in the NE–SW, N–S, and E–W directions, which agrees with the previous studies [21,22].

However, aeromagnetic method results showed that the magnetic intensity values ranged between −431.38 nT for magnetic low and 399.82 nT for magnetic high, with RTP map magnetic intensity ranging from −416.45 to 664.45 nT. The FVD map showed magnetic intensity values which ranged from −0.5863 to 0.9060 nT/km^2. The total horizontal derivative map intensity ranged from −0.00031 to 0.762691 nT/km^2 while the analytical map showed magnetic intensity ranging from

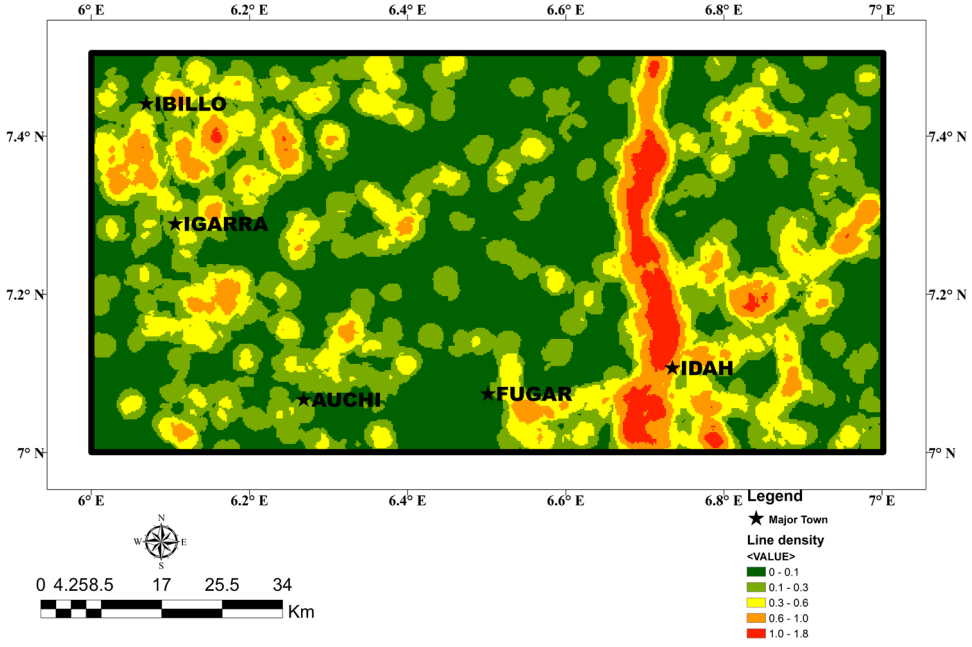

Figure 19: Lineament density map of the study area.

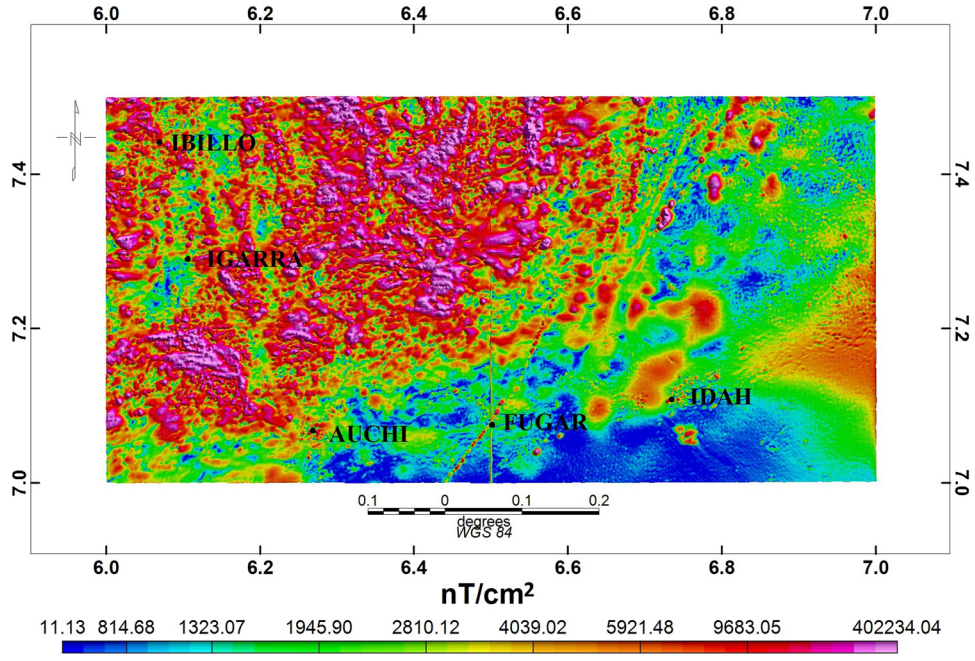

Figure 20: Analytical signal map of the study area.

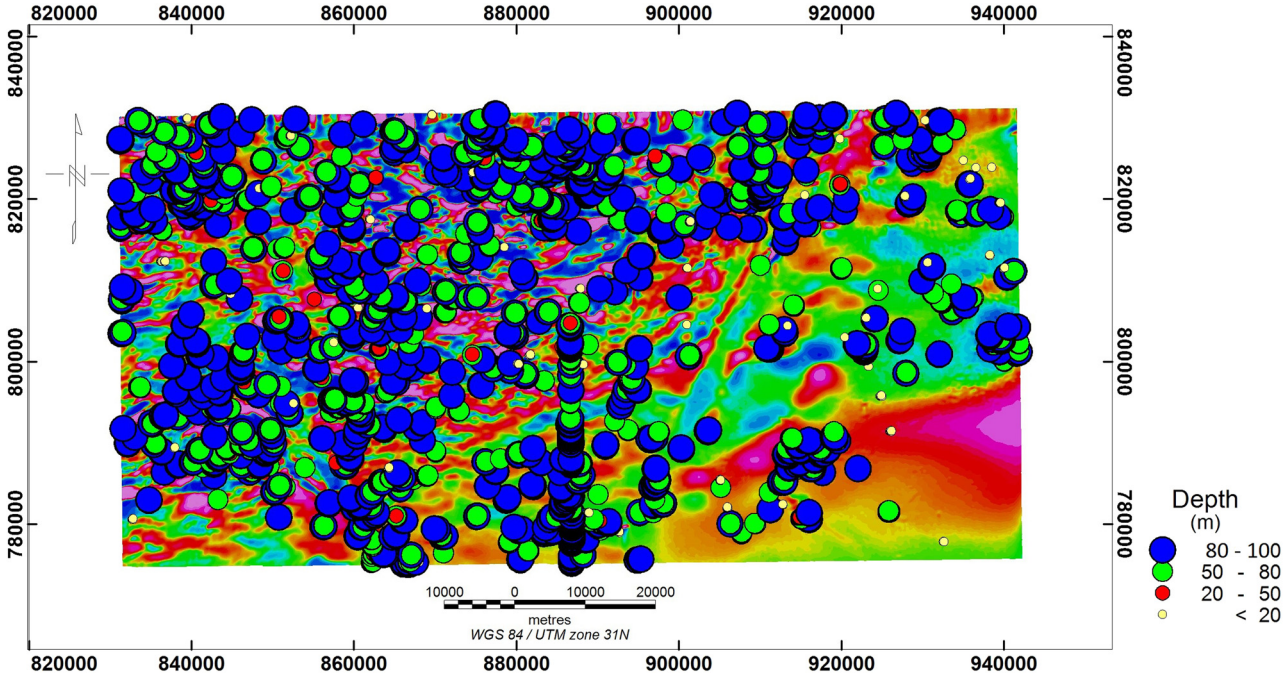

Figure 21: Windowed Euler deconvolution depth to magnetic source (100 m).

−14.0664 to 394607.3438 nT/cm^2. The windowed Euler deconvolution depth to magnetic source showed depth range of <20 to 2,000 m. The results also show the major lithological boundary between the basement and sedimentary rocks in the area. Various structures were deduced from the first, second, and total vertical and horizontal derivative maps of the area. These structures are a product of tectonism and their various orientations agree with the findings from previous research in the area. For example, areas characterised by iron oxide alteration are the most suitable for gold exploration due to various hydrothermally altered structures, which is in line with the works of Ejepu

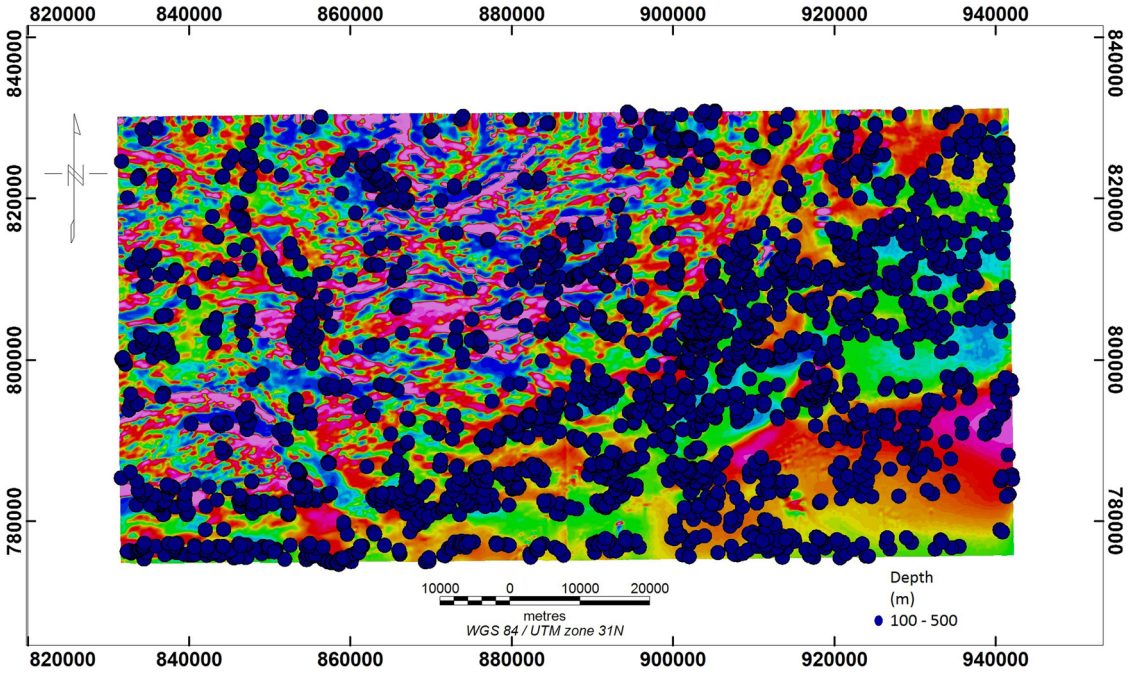

Figure 22: Windowed Euler deconvolution depth to magnetic source (500 m).

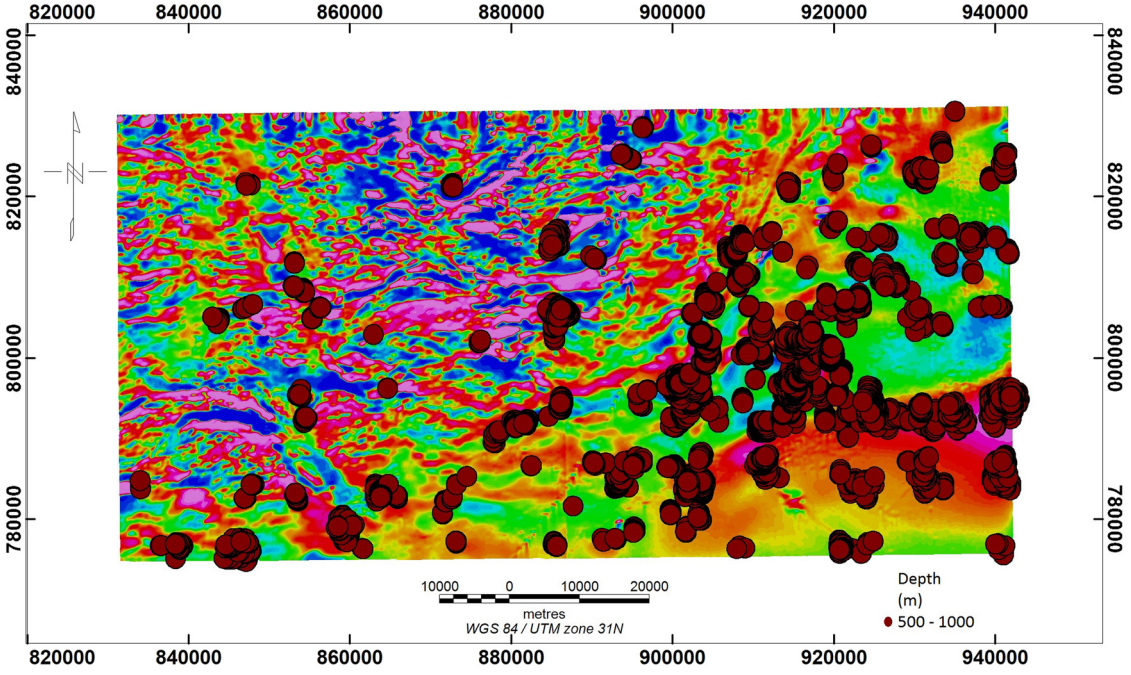

Figure 23: Windowed Euler deconvolution depth to magnetic source (1,000 m).

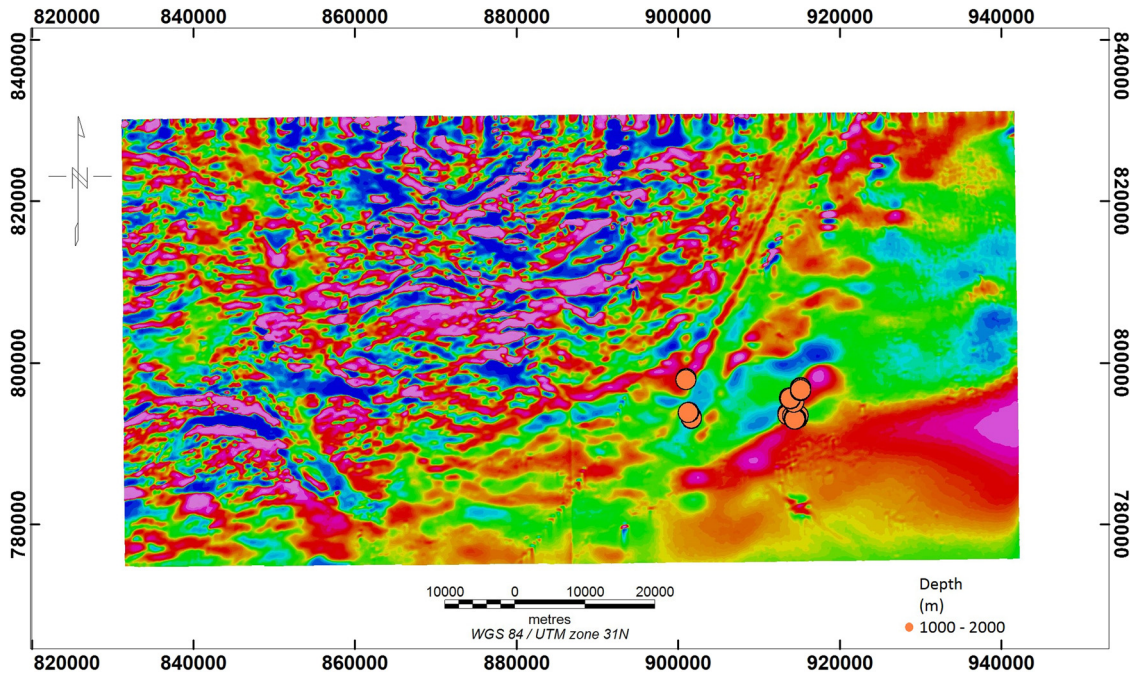

Figure 24: Windowed Euler deconvolution depth to magnetic source (2,000 m).

et al. [26]. Also, clay alteration zones sometimes are regions where mineralized pegmatites are weathered, which agrees with the work of Obaje [27]. Based on the findings of this research, it is concluded that the area of study has huge mineral exploration potential and it is not surprising that various deposits have been recorded already, which include iron ore, marble, coal, and kaolinite.

Acknowledgement: This is to appreciate Covenant University Centre for Research Innovation and Discovery (CUCRID) and Covenant University as a whole for their financial support towards this study.

Author contributions: O.A.O. developed the concept, methodology, and worked on formal analysis, resources, data curation, writing – original draft, visualisation, and writing – review and editing. H.O.B. worked on methodology and review. S.A.A. worked on data curation and methodology. A.P.A. worked on the grammatical errors.

Conflict of interest: The authors state no conflict of interest.

References

[1] Adagunodo TA, Sunmonu LA, Adetunji AA. An overview of magnetic method in mineral exploration. J Glob Ecol Environ. 2015;3(1):13–28.

[2] Olasunkanmi NK, Sunmonu LA, Adabanija MA, Oladejo PO. Interpretation of high resolution aeromagnetic data for mineral prospect in Igbeti-Moro area, southwestern Nigeria. IOP Conf Ser Earth Environ Sci. 2018;173(1):1–9. doi: 10.1088/1755-1315/173/1/012033.

[3] Amadikwa LO, Selemo AI, Obioha YE, Okorie OJ. Application of aeromagnetic data for mineral exploration in Igarra and environs, southwestern Nigeria. Int J Adv Acad Res. 2019;5(10):10–25.

[4] Obiora DN, Okorie AC. Spectral analysis and modeling of magnetic anomalies in part of northern Anambra basin, Nigeria. Environ Res J. 2020;14(3):84–96.

[5] Okorie AC, Obiora DN, Igwe E. Geophysical study of Ubiaja and Illushi area in northern Anambra basin, Nigeria, using combined interpretation methods of aeromagnetic data. Model Earth Syst Environ. 2019;5(3):1071–82. doi: 10.1007/s40808-019-00592-0.

[6] Asadu AN, Ibe KA. Petroleum geology of outcropping sediments along Imiegba road in etsako east local government area of Edo state, southern Anambra basin flank, Nigeria: inference from sedimentology and organic geochemistry. J Geogr Environ Earth Sci Int. 2017;10(3):1–10. doi: 10.9734/JGEESI/2017/33891.

[7] Onu KF. The Southern Benue trough and Anambra Basin, Southeastern Nigeria: A stratigraphic review. J Geogr Environ Earth Sci Int. 2017;12(2):1–16. doi: 10.9734/JGEESI/2017/30416.

[8] Igbinigie N, Akenzua A. Palynological studies of maastrichtian to Paleocene sediments exposed at Okpekpe, western flank of Anambra basin, Edo state, Nigeria. J Appl Sci Environ Manag. 2018;22(10):1563–6. doi: 10.4314/jasem.v22i10.05.

[9] Yusuf I, Ogundele JO, Odejobi Y, Auwal HI. Geophysical investigation of loss of circulation in borehole drilling: A case study of Auchi polytechnic. Int J Sci Tech Soc. 2015;3(3):90–5. doi: 10.11648/j.ijsts.20150303.14.

[10] Oladejo OP, Adagunodo TA, Sunmonu LA, Adabanija MA, Omeje M, Babarimisa IO, et al. Structural analysis of subsurface stability

using aeromagnetic data: a case of Ibadan, southwestern Nigeria. J Phys Conf Ser. 2019;1299(1):012083.
[11] Oni OA, Aizebeokhai AP. Aeromagnetic data processing using MATLAB. IOP Conf Ser Earth Environ Sci. 2022;993(1):012017.
[12] Luo Y, Xue DJ, Wang M. Reduction to the pole at the geomagnetic equator. Chin J Geophys. 2010;53(6):1082–9.
[13] Geosoft Inc. Oasis Montaj Version 7.0.1 User Guide. Toronto: Geosoft Incorporated; 2008.
[14] Ku CC, Sharp JA. Werner deconvolution for automated magnetic interpretation and its refinement using Marquart's inverse modelling. Geophysics. 1983;48(6):754–74. doi: 10.1190/1.1441505.
[15] Osinowo OO, Olayinka AI. Aeromagnetic mapping of basement topography around the Ijebu-Ode geological transition zone, Southwestern Nigeria. Acta Geod Geophys. 2013;48(4):451–70.
[16] Cooley T, Anderson GP, Felde GW, Hoke ML, Ratkowski AJ, Chetwynd JH, et al. FLAASH, a MODTRAN4-based atmospheric correction algorithm, its application and validation. International Geoscience and Remote Sensing Symposium. Vol. 3. 2002. p. 1414–8.
[17] Clark RN, Swayze GA. Mapping minerals, amorphous materials, environmental materials, vegetation, water, ice, and snow, and other materials: The USGS Tricorder Algorithm. In: Summaries of the Fifth Annual JPL Airborne Earth Science Workshop. Vol. 1. JPL Publication; 1995. p. 39–40.
[18] Clark RN, Swayze GA, Gallagher A, King TVV, Calvin WM. The U.S. Geological Survey, Digital Spectral Library: Version 1: 0.2 to 3.0 microns: U.S. Geological Survey Open File Report 93-592; 1993. p. 1340. http://speclab.cr.usgs.gov.
[19] Pour AB, Park Y, Park TYS, Hong JK, Hashim M, Woo J, et al. Regional geology mapping using satellite-based remote sensing approach in Northern Victoria Land, Antarctica. Polar Sci. 2018;16:23–46.
[20] Sabins Jr FF. Remote sensing - Principles and interpretation. New York: Freeman; 1987.
[21] Ogbe OB, Olobaniyi SB, Ejeh OI, Omo-Irabor OO, Osokpor J, Ocheli A, et al. Petrological and structural investigation of rocks around Igarra, southwestern Nigeria. Ife J Sci. 2018;20(3):663–77.
[22] Ajigo IO, Odeyemi IB, Ademeso OA. Field geology and structures of migmatitic gneisses around Ibillo-Okene area, Southwest Nigeria. J Environ Earth Sci. 2019;9(2):59–72. doi: 10.7176/JEES/9-2-08.
[23] Onwuemesi AG. One dimensional spectral analysis of aeromagnetic anomalies and curie depth isotherm in Anambra basin of Nigeria. J Geodyn. 1997;23(2):95–107.
[24] Onuba LN, Anudu GK, Chiaghanam OI, Anakwuba EK. Evaluation of aeromagnetic anomalies over Okigwe Area, Southern Nigeria. Res J Environ Earth Sci. 2011;3(5):498–507.
[25] Onwe IM, Odoh BI, Onwe RM. Estimation of sedimentary thickness in eastern Anambra basin by qualitative and quantitative interpretation of aeromagnetic data. Adv Appl Sci Res. 2015;6(10):1–6.
[26] Ejepu JS, Ako TA, Abdullahi S. Integrated geosciences prospecting for gold mineralization in Kwakuti, North-Central Nigeria. J Geol Min Res. 2018;10(7):81–94.
[27] Obaje NG. Geology and mineral resources of Nigeria. Vol. 120. Berlin Heidelberg: Springer-Verlag; 2009. p. 15.